nanomaterials

MDPI

Communication

Surface Degradation Mechanism on $CH_3NH_3PbBr_3$ Hybrid Perovskite Single Crystal by a Grazing E-Beam Irradiation

Heriyanto Syafutra [1], Jung-Ho Yun [2,*], Yuya Yoshie [1], Miaoqiang Lyu [2], Sakura Nishino Takeda [1], Masakazu Nakamura [1], Lianzhou Wang [2,*] and Min-Cherl Jung [3,*]

1 Division of Materials Science, Nara Institute of Science and Technology, Nara 630-0192, Japan; heriyanto.syafutra.hi0@ms.naist.jp (H.S.); yoshie.yuya.ys9@ms.naist.jp (Y.Y.); sakura@ms.naist.jp (S.N.T.); mnakamura@ms.naist.jp (M.N.)
2 Nanomaterials Centre, School of Chemical Engineering and Australian Institute for Bioengineering and Nanotechnology (AIBN), University of Queensland, QLD 4072, Australia; m.lyu@uq.edu.au
3 Division of Materials Science, Faculty of Pure and Applied Sciences, University of Tsukuba, Ibaraki 305-8577, Japan
* Correspondence: j.yun1@uq.edu.au (J.-H.Y.); l.wang@uq.edu.au (L.W.); jung.mincherl.fp@u.tsukuba.ac.jp (M.-C.J.); Tel.: +81-29-853-4995 (M.-C.J.)

Received: 1 June 2020; Accepted: 23 June 2020; Published: 28 June 2020

Abstract: To start a step such as some realization of minimized and integrated devices, it requires simply understanding the surface status of hybrid perovskite on the e-beam irradiation because many commercial semiconductor devices are performed with a surface patterning process using e-beam or etching gas. The surface status of $CH_3NH_3PbBr_3$ ($MAPbBr_3$) single crystal was studied after a grazing e-beam irradiation in an ultra-high vacuum. The prepared hybrid perovskite single crystal was irradiated by the 3 degree-grazing e-beam with energy of 15 kV for 10 min using a reflection high-electron energy diffraction technique. The e-beam irradiation on the $MAPbBr_3$ hybrid perovskite single crystal induced the deformation from $MAPbBr_3$ into MABr, Br_2, and Pb on the surface. The gas phases of MABr and Br_2 are depleted from the surface and the Pb element has remained on the surface. As a result of the e-beam irradiation, it formed a polycrystalline-like phase and Pb metal particles on the surface, respectively.

Keywords: surface degradation; $MAPbBr_3$ single crystal; grazing e-beam radiation

1. Introduction

Recently, organic-inorganic hybrid perovskite (OHP) materials have shown impressive results, especially in the case of solar cells, including a power conversion efficiency of over 25%, because of their key physical properties such as high absorption coefficient, high carrier mobility, and long carrier lifetime [1–4]. However, there are attempts to overcome the critical problems such as material instability and environmental issues caused by Pb-based perovskite, due to which the research on OHP materials is still focused on the solar cell application [5–7]. In the case of materials instability, particularly, the degradation of OHP materials under electron beam, UV (ultra-violet), and visible light illumination conditions has been reported [6–11]. C. Xiao, et al. had reported the two-steps degradation mechanism such as (1) defect formation caused by irradiation damage and (2) phase transformation induced by electron-beam heating with a high-energy electron beam (5 and 10 kV) [7]. Additionally, the e-beam effect exposed with the perpendicular direction between the e-beam and the hybrid perovskite layer was reported by N. Klein-Kedem, et al. to explain the degradation of the perovskite structure [8].

Interestingly, these reports show the behavior on the bulk status in solar-cell device structures because the e-beam was exposed only to the active hybrid perovskite area in a device structure. This approach would be a reasonable to understand the damage effects induced by several variables such as the local heat and radiation damage in the solar-cell application field. However, there is no serious study on the surface status of hybrid perovskite materials by the e-beam irradiation yet. If we try to make a designed pattern on the surface of hybrid perovskite materials using the e-beam irradiation which is a useful and conventional tool in the semiconductor industrials, its effect on the surface should be studied firstly.

In the last decade, researchers have started exploring the possibility of new applications using hybrid perovskite materials such as optoelectronics, memory, laser, THz application, transistor, sensors, and batteries, alongside with specific researches on defects, phonon, and electronic structures, which can be important fundamentals to support future perovskite-applied research [12–21]. At the same time, we believe that it requires to start a next step such as some realization of minimized and integrated devices needed in the semiconductor industrials [22]. To perform this next step, the etching (or patterning) method and its effect on the surface of active material should be firstly studied. The e-beam is one of candidates for etching (or patterning) and we need to understand the surface status of hybrid perovskite on the e-beam irradiation for etching (or patterning).

In this short communication, we have studied the surface status of the hybrid perovskite single crystal, $CH_3NH_3PbBr_3$ ($MAPbBr_3$), by a grazing e-beam irradiation with high energy. Also, the surface degradation in the hybrid perovskite material is discussed with the remaining Pb particles and the polycrystalline-like phase.

2. Materials and Methods

$MAPbBr_3$ single crystal was grown by an inverse temperature method [23]. A $MAPbBr_3$ precursor solution (1.2 M) was prepared by mixing MABr and $PbBr_2$ (1:1 molar ratio) in dimethylformamide (DMF). After 30 min of stirring, the solution was filtered through a 0.2 mm pore-size polytetrafluoroethylene (PTFE) syringe filter, and the filtered precursor solution was gradually heated to 90 °C using an oil-bath. Several hundred micron-sized single seed crystals were formed within 1 h. Large-sized (centimeter scale) single crystals were prepared through a crystallization process over 24 h by use of the chosen seed crystals with regular changes of the precursor solution. (Figure 1a)

For a grazing e-beam irradiation on the surface of a single crystal, we used an electron gun in a reflection high-energy electron diffraction (RHEED) system. Before and after loading the sample to the RHEED chamber, we performed the surface scratching using a knife and the annealing process at 100 °C for 10 min, respectively [24]. The base pressure of the RHEED chamber was 1.1×10^{-9} Torr. The energy, current, and incident angle were 15 kV, 20 μA, and 3 deg., respectively (Figure 1b). After irradiating for 10 min, we took out the sample and then performed atomic force microscopy (AFM), scanning electron microscopy (SEM), X-ray diffraction (XRD), and high-resolution X-ray photoelectron spectroscopy (XPS). We performed the AFM measurement using SPM-9700 made by Shimazu (Kyoto, Japan). The used SEM system is the HITACHI SU9000 model (Krefeld, Germany) with the acceleration voltage of 5.0 kV and the emission current of 10 μA. The XRD is RINT-TTRIII/NM with CuK_α source made by Rigaku (Tokyo, Japan). We used the Versa ProbeII with a monochromated AlK_α (ULVAC-PHI, Kanagawa, Japan) for all XPS measurements and obtained the C 1*s*, N 1*s*, Pb 4*f*, and I 4*d* core-level spectra. The binding energies were calibrated with reference to the Au $4f_{7/2}$ level (84.0 eV) [25].

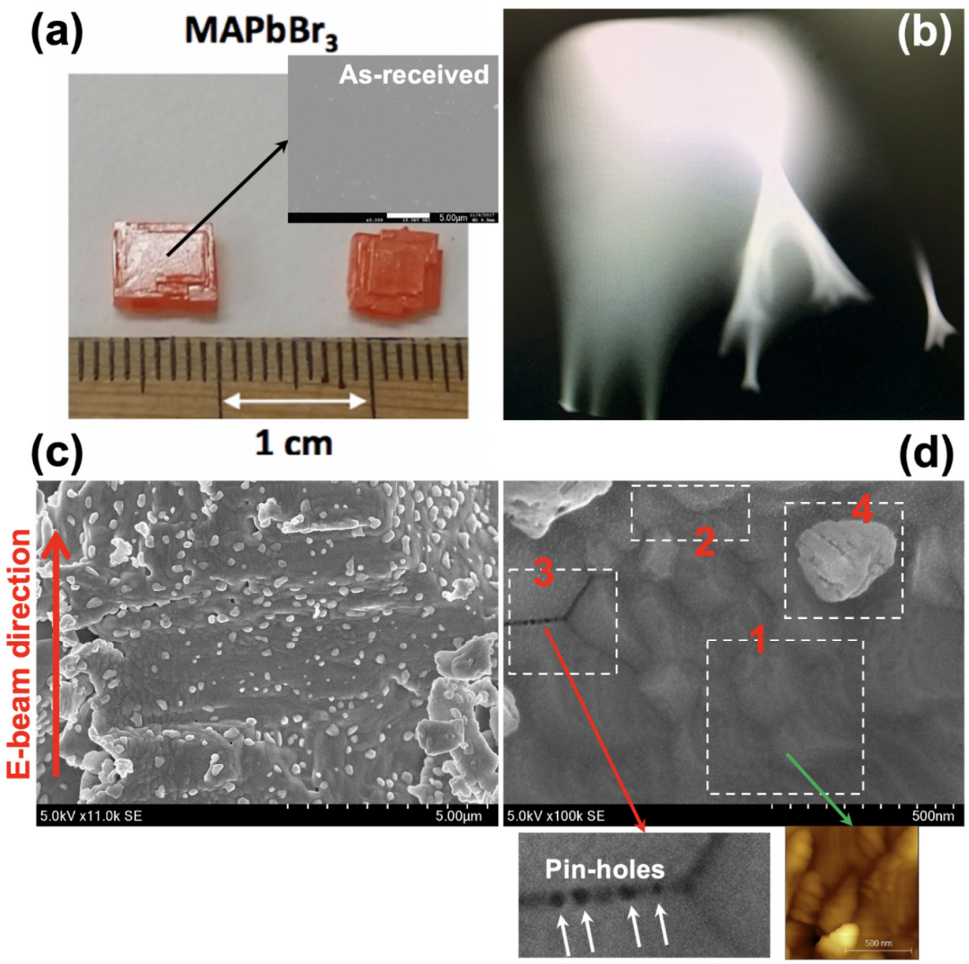

Figure 1. (**a**) The prepared $MAPbBr_3$ single crystals with the diameter of 0.6 cm. In the scanning electron microscopy (SEM) measurement for the as-received sample (before the e-beam irradiation), it shows very flat surface. (**b**) The reflection high-energy electron diffraction (RHEED) screen with no spots. It shows a dynamic flowing on the screen. (**c**) The top surface morphology measured by SEM. The recessed surface irradiated by the grazing e-beam and many particles on the surface were observed. (**d**) the four different features (the red numbers) are observed. In the 1 and 3 areas, interestingly, the steps (measured by atomic force microscopy (AFM)) and pin-holes are clearly observed.

3. Results and Discussion

Interestingly, the dynamic flowing on the screen of RHEED was observed without any atomic patterns or spots [26] (Figure 1b). It might be due to a surface charging effect, and the similar results have been reported before [6–8].

With the SEM measurement, many small particles and steps have been observed on the surface (Figure 1c) where four patterns on the surface have been shown on the following locations in Figure 1d: location 1) many steps (indicated by the green arrow toward an inset AFM topology image), location 2) large surface roughness, location 3) pinholes/deep boundary (the white arrow), and location 4) particles. (Figure 1d) The e-beam irradiation on the $MAPbBr_3$ single crystal seems to cause a polycrystalline-like phase by degradation. It is assumed that these findings can be employed to understanding a degradation mechanism of $MAPbBr_3$, processing from location 1 to location 4 in sequence. Firstly, steps and valleys start appearing on the surface. Secondly, the height between steps becomes larger and larger. And then the pinholes occur on the step boundary while forming a grain boundary. Finally, the one grain is isolated and remains a particle. To confirm this assumption, it is required to know its atomic structure and chemical state in bulk and surface, respectively.

To see the bulk status after the grazing e-beam irradiation, we performed an XRD experiment (Figure 2a). Only the typical $MAPbBr_3$ structure was observed and there was no other significant structure [27]. With this result, we confirmed the irradiation effect of the e-beam was only affected on the surface.

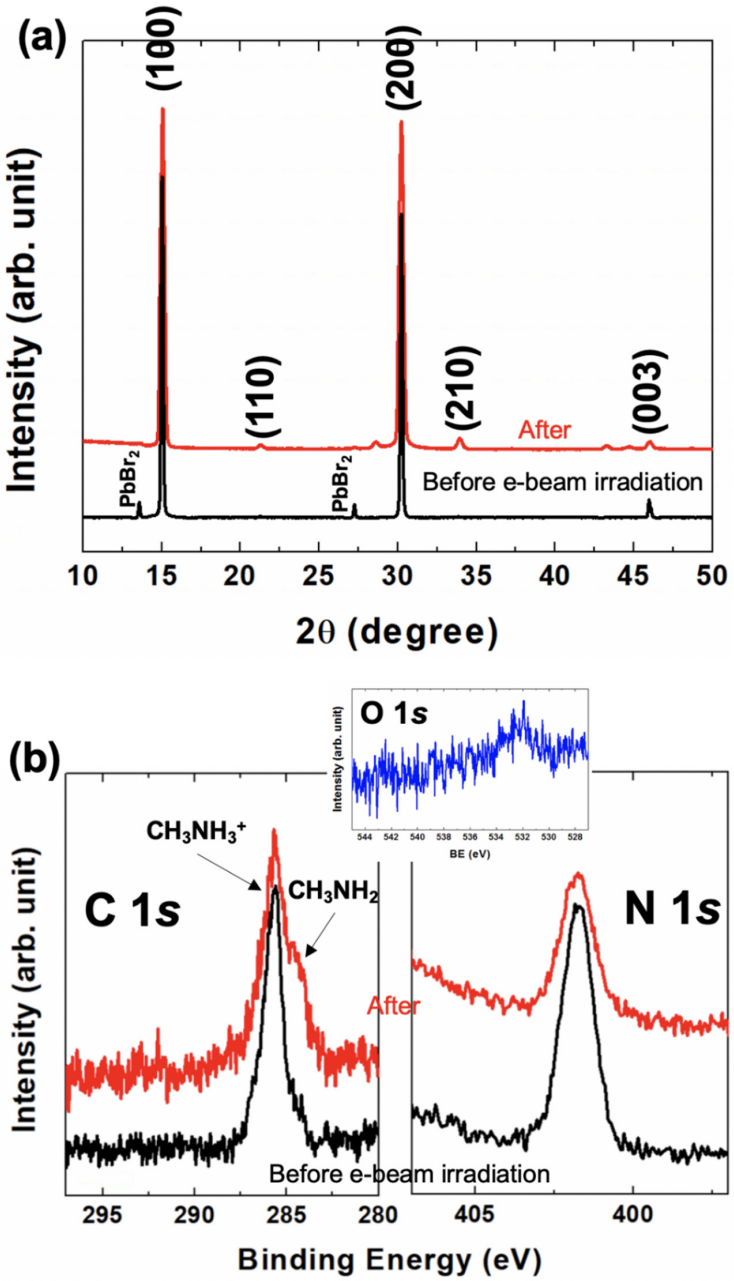

Figure 2. (**a**) The X-ray diffraction (XRD) result before and after the grazing e-beam irradiation. The as-received sample still shows the small $PbBr_2$ peak. After the e-beam irradiation, however, it was disappeared. (**b**) The C, N, and O 1*s* core-level spectra before and after the e-beam irradiation. The CH_3NH_2 molecular defect has appeared after the e-beam irradiation [28,29]. This defect is due to the formation of a polycrystalline-like phase on the surface [29]. The O 1*s* core-level peak is appeared slightly at around 532 eV which is shown with the physiosorbed oxygen on the surface.

To see the detailed changes on the surface, XPS was measured with C 1*s*, N 1*s*, Pb 4*f*, and Br 3*d* core-level spectra. (Figures 2b and 3) Also, we measured O 1*s* core-level to confirm the surface contamination after taking out the sample from the RHEED chamber (Figure 2b). The peak with

a small trace was observed. If this O 1*s* peak has some chemical bonding with carbon, nitrogen, or other elements, we would observe some different chemical states in C, N 1*s*, Pb 4*f*, or Br 3*d* core-level spectra [25]. However, we could not observe any significant change of chemical states in the C and N 1*s* core-level spectra (Figure 2b). The binding energies of C and N 1*s* core-levels are the same as those of our several previous studies that showed only the hybrid perovskite state [28,29]. It means that oxygen contamination does not make any chemical states bonded to $CH_3NH_3^+$ cation. Interestingly, we found the Pb^{0+} chemical state (Pb metal) in the Pb 4*f* core-level spectrum (Figure 3a). However, we could not observe any significant chemical state except for the hybrid perovskite state. The single chemical state in the Br 3*d* core-level was confirmed by the curve fitting which was performed with Doniach-Sŭnjić curves, convoluted with a Gaussian distribution function, considering instrumental broadening and background noise due to inelastic scattering was subtracted by the Shirley (integral) method (Figure 3b) [30,31].

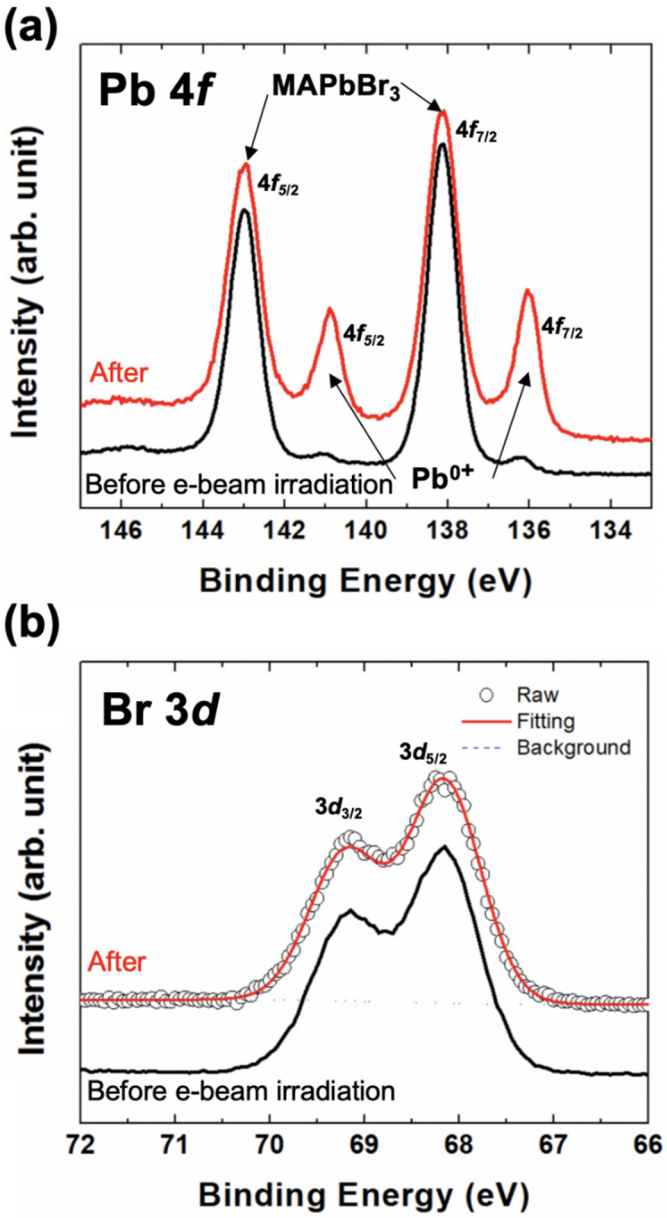

Figure 3. (**a**) The Pb 4*f* core-level spectra before and after the grazing e-beam irradiation. The Pb^{0+} chemical state is clearly observed. (**b**) After the curve fitting, the Br 3*d* core-level spectra before and after the grazing e-beam irradiation shows the single chemical state perfectly.

With these results, we can confirm three important facts—(1) the particles on the surface are pure Pb metal, (2) the surface has no oxide state (which means the surface oxygen is a physical-absorption state), and (3) the surface degradation is occurred by the e-beam irradiation. (Equation (1))

$$MAPbBr_3\ (\text{single crystal}) \rightarrow MABr \uparrow + Br_2 \uparrow + Pb\ (\text{on the surface}) \quad (1)$$

As a result of grazing e-beam irradiation, the chemical bonding is broken first and then two gas phases, such as MABr and Br_2, are depleted from the surface. The Pb metal only remains on the surface with the particle structure. The surface becomes the polycrystalline-like phase from the single crystal phase. These understandings are similar to two reports by Z. Dang, et al. and A. Kostopoulou, et al. in all-inorganic halide perovskite materials [10,32]. However, in the case of organic-inorganic hybrid perovskite material, it shows that no remained molecular parts on the surface because of its surface depletion.

4. Conclusions

We observed the surface degradation of $MAPbBr_3$ single crystal using the 3 degree-grazing e-beam irradiation with the 15-kV high energy. The e-beam irradiation causes the destruction of the chemical structure of $MAPbBr_3$ without creating any different chemical states such as etching. However, the Pb metal element with the form of particles remains on the surface. If we use a focused and well-defined sized e-beam, it will be possible to make a designed pattern of an organic-inorganic hybrid perovskite main layer with Pb metal capper or wire on the surface. This experimental idea is suggested for future work.

Author Contributions: M.-C.J. conceived the idea, designed the experiments, and supervised the project. H.S., M.L., and J.-H.Y. performed a major portion of the sample preparation and characterization. Y.Y. and S.N.T. performed the RHEED experiment. All authors discussed the results, performed data analysis and explanation, wrote the manuscript, and revised it. All authors have read and agreed to the published version of the manuscript.

Funding: This work was supported by funding from Faculty of Pure and Applied Sciences in University of Tsukuba (Japan). This work was also supported by the Australia Research Council through its DECRA and DP programs.

Conflicts of Interest: The authors declare no conflict of interest.

References

1. Green, M.A.; Ho-Baillie, A.; Snaith, H.J. The emergence of perovskite solar cells. *Nat. Photonics* **2014**, *8*, 506–514. [CrossRef]
2. Lin, J.; Lai, M.; Dou, L.; Kley, C.S.; Chen, H.; Peng, F.; Sun, J.; Lu, D.; Hawks, S.A.; Xie, C.; et al. Thermochromic halide perovskite solar cells. *Nat. Mater.* **2018**, *17*, 261–267. [CrossRef] [PubMed]
3. Green, M.A.; Bremner, S.P. Energy conversion approaches and materials for high-efficiency photovoltaics. *Nat. Mater.* **2016**, *16*, 23–34. [CrossRef]
4. Snaith, H. Perovskites: The emergence of a new era for low-cost, high-efficiency solar cells. *J. Phys Chem. Lett.* **2013**, *4*, 3623–3630. [CrossRef]
5. Lee, Y.M.; Park, J.; Yu, B.D.; Hong, S.; Jung, M.C.; Nakamura, M. Surface instability of Sn-based hybrid perovskite thin film, $CH_3NH_3SnI_3$: The origin of its material instability. *J. Phys. Chem. Lett.* **2018**, *9*, 2293–2297. [CrossRef] [PubMed]
6. Docampo, P.; Bein, T. A long-term view on perovskite optoelectronics. *Acc. Chem. Res.* **2016**, *49*, 339–346. [CrossRef] [PubMed]
7. Xiao, C.; Li, Z.; Guthrey, H.; Moseley, J.; Yang, Y.; Wozny, S.; Moutinho, H.; To, B.; Berry, J.J.; Gorman, B.; et al. Mechanisms of electron-beam-induced damage in perovskite thin films revealed by cathodoluminescence spectroscopy. *J. Phys. Chem. C* **2015**, *119*, 26904–26911. [CrossRef]
8. Klein-Kedem, N.; Cahen, D.; Hodes, G. Effects of light and electron beam irradiation on halide perovskites and their solar cells. *Acc. Chem. Res.* **2016**, *49*, 347–354. [CrossRef] [PubMed]

9. Dang, Z.; Shamsi, J.; Akkerman, Q.A.; Imran, M.; Bertoni, G.; Brescia, R.; Manna, L. Low-temperature electron beam-induced transformations of cesium lead halide perovskite nanocrystals. *ACS Omega* **2017**, *2*, 5660–5665. [CrossRef] [PubMed]
10. Dang, Z.; Shamsi, J.; Palazon, F.; Imran, M.; Akkerman, Q.A.; Park, S.; Bertoni, G.; Prato, M.; Brescia, R.; Manna, L. In situ transmission electron microscopy study of electron beam-induced transformations in colloidal cesium lead halide perovskite nanocrystals. *ACS Nano* **2017**, *11*, 2124–2132. [CrossRef]
11. Pérez-Robles, S.; Matute, C.A.; Lara, J.R.; Lopera, S.H.; Cortés, F.B.; Franco, C.A. Effect of nanoparticles with different chemical nature on the stability and rheology of acrylamide sodium acrylate copolymer/chromium (III) acetate gel for conformance control operations. *Nanomaterials* **2019**, *10*, 74. [CrossRef] [PubMed]
12. Jia, Y.; Kerner, R.A.; Grede, A.J.; Rand, B.P.; Giebink, N.C. Continuous-wave lasing in an organic–inorganic lead halide perovskite semiconductor. *Nat. Photonics* **2017**, *11*, 784–788. [CrossRef]
13. Sun, J.; Wu, J.; Tong, X.; Lin, F.; Wang, Y.; Wang, Z.M. Organic/inorganic metal halide perovskite optoelectronic devices beyond solar cells. *Adv. Sci.* **2018**, *5*, 1700780. [CrossRef] [PubMed]
14. Hoye, R.L.Z.; Schulz, P.; Schelhas, L.T.; Holder, A.M.; Stone, K.H.; Perkins, J.D.; Vigil-Fowler, D.; Siol, S.; Scanlon, D.O.; Zakutayev, A.; et al. Perovskite-Inspired Photovoltaic Materials: Toward Best Practices in Materials Characterization and Calculations. *Chem. Mater.* **2017**, *29*, 1964–1988. [CrossRef]
15. Lee, Y.M.; Yun, J.H.; Matsuyama, A.; Kobori, S.; Maeng, I.; Lyu, M.; Wang, S.; Wang, L.; Jung, M.C.; Nakamura, M. Significant THz-wave absorption property in mixed δ- And α-$FAPbI_3$ hybrid perovskite flexible thin film formed by sequential vacuum evaporation. *Appl. Phys. Express* **2019**, *12*, 051003. [CrossRef]
16. Maeng, I.; Lee, Y.M.; Park, J.; Raga, S.R.; Kang, C.; Kee, C.S.; Yu, B.D.; Hong, S.; Ono, L.K.; Qi, Y.; et al. Significant THz absorption in CH_3NH_2 molecular defect-incorporated organic-inorganic hybrid perovskite thin film. *Sci. Rep.* **2019**, *9*, 5811. [CrossRef]
17. Senanayak, S.P.; Yang, B.; Thomas, T.H.; Giesbrecht, N.; Huang, W.; Gann, E.; Nair, B.; Goedel, K.; Guha, S.; Moya, X.; et al. Understanding charge transport in lead iodide perovskite thin-film field-effect transistors. *Sci. Adv.* **2017**, *3*, e1601935. [CrossRef]
18. Brintakis, K.; Gagaoudakis, E.; Kostopoulou, A.; Faka, V.; Argyrou, A.; Binas, V.; Kiriakidis, G.; Stratakis, E. Ligand-free all-inorganic metal halide nanocubes for fast, ultra-sensitive and self-powered ozone sensors. *Nanoscale Adv.* **2019**, *1*, 2699–2706. [CrossRef]
19. Stoeckel, M.-A.; Gobbi, M.; Bonacchi, S.; Liscio, F.; Ferlauto, L.; Orgiu, E.; Samorì, P. Reversible, fast, and wide-range oxygen sensor based on nanostructured organometal halide perovskite. *Adv. Mater.* **2017**, *29*, 1702469. [CrossRef]
20. Kostopoulou, A.; Vernardou, D.; Savva, K.; Stratakis, E. All-inorganic lead halide perovskite nanohexagons for high performance air-stable lithium batteries. *Nanoscale* **2019**, *11*, 882–889. [CrossRef]
21. Kostopoulou, A.; Brintakis, K.; Nektarios, K. Nasikas and Emmanuel Stratakis Perovskite nanocrystals for energy conversion and storage in: Nanophotonics Volume 8 Issue 10 (2019). *Nanophotonics* **2019**, *8*, 1607–1640. [CrossRef]
22. Chou, S.S.; Swartzentruber, B.S.; Janish, M.T.; Meyer, K.C.; Biedermann, L.B.; Okur, S.; Burckel, D.B.; Carter, C.B.; Kaehr, B. Laser Direct Write Synthesis of Lead Halide Perovskites. *J. Phys. Chem. Lett.* **2016**, *7*, 3736–3741. [CrossRef] [PubMed]
23. Saidaminov, M.I.; Abdelhady, A.L.; Murali, B.; Alarousu, E.; Burlakov, V.M.; Peng, W.; Dursun, I.; Wang, L.; He, Y.; MacUlan, G.; et al. High-quality bulk hybrid perovskite single crystals within minutes by inverse temperature crystallization. *Nat. Commun.* **2015**, *6*, 1–6. [CrossRef] [PubMed]
24. Ohmann, R.; Ono, L.K.; Kim, H.S.; Lin, H.; Lee, M.V.; Li, Y.; Park, N.G.; Qi, Y. Real-space imaging of the atomic structure of organic-inorganic perovskite. *J. Am. Chem. Soc.* **2015**, *137*, 16049–16054. [CrossRef] [PubMed]
25. Wagner, C.D.; Riggs, W.M.; Davis, L.E.; Moulder, J.F.; Muilenberg, G.E. *Handbook of X-ray Photoelectron Spectroscopy*: A Reference Book of Standard Spectra for Identification and Interpretation of XPS Data-Catalog-UW-Madison Libraries; Physical Electronics: Chanhassen, MN, USA, 1995; ISBN-13 9780964812413, ISBN-10 096481241X.
26. Jung, M.C.; Kobori, S.; Matsuyama, A.; Maeng, I.; Lee, Y.M.; Kojima, H.; Benten, H.; Nakamura, M. Formation of CH_3NH_2-incorporated intermediate state in $CH_3NH_3PbI_3$ hybrid perovskite thin film formed by sequential vacuum evaporation. *Appl. Phys. Express* **2019**, *12*, 015501. [CrossRef]
27. Hasegawa, S. Reflection high-energy electron diffraction. In *Characterization of Materials*; John Wiley & Sons, Inc.: Hoboken, NJ, USA, 2012; pp. 1–14.

28. Jung, M.C.; Lee, Y.M.; Lee, H.K.; Park, J.; Raga, S.R.; Ono, L.K.; Wang, S.; Leyden, M.R.; Yu, B.D.; Hong, S.; et al. The presence of CH_3NH_2 neutral species in organometal halide perovskite films. *Appl. Phys. Lett.* **2016**, *108*, 073901. [CrossRef]
29. Wang, K.H.; Li, L.C.; Shellaiah, M.; Sun, K.W. Structural and photophysical properties of methylammonium lead tribromide ($MAPbBr_3$) single crystals. *Sci. Rep.* **2017**, *7*, 1–14. [CrossRef]
30. Doniach, S.; Sunjic, M. Many-electron singularity in X-ray photoemission and X-ray line spectra from metals. *J. Phys. C Solid State Phys.* **1970**, *3*, 285–291. [CrossRef]
31. Shirley, D.A. High-resolution x-ray photoemission spectrum of the valence bands of gold. *Phys. Rev. B* **1972**, *5*, 4709–4714. [CrossRef]
32. Kostopoulou, A.; Sygletou, M.; Brintakis, K.; Lappas, A.; Stratakis, E. Low-temperature benchtop-synthesis of all-inorganic perovskite nanowires. *Nanoscale* **2017**, *9*, 18202–18207. [CrossRef]